Product rotational distributions and specific opacity functions for the reaction Ba + HI → BaI (v=0,4,8,12,16,18) + H

A. A. Tsekouras,[a] C. A. Leach,[b] K. S. Kalogerakis, and R. N. Zare[c]
Department of Chemistry, Stanford University, Stanford, California 94305

(Received 26 June 1992; accepted 6 August 1992)

The reaction Ba+HI→BaI(v)+H was studied under beam-gas, single-collision conditions with an average center-of-mass collision energy of 13 kJ mol^{-1}. BaI (v) rotational distributions were recorded for v=0, 4, 8, 12, 16, and 18 by means of selectively detected laser-induced fluorescence of the BaI $C\,^2\Pi$–$X\,^2\Sigma^+$ band system. Each rotational distribution exhibits a maximum toward its high energy end and the range of rotational states becomes narrower as product vibration increases. Because the kinematic constraint causes almost all reagent orbital angular momentum to appear in product rotation, the principle of angular momentum conservation provides the means for determining specific opacity functions from the rotational distributions and the reagent relative velocity distribution. The specific opacity functions are narrow functions of the impact parameter. The peak values decrease smoothly from approximately 4.5 Å for v=0 to 1.5 Å for v=18, indicating a strong correlation between impact parameter and product vibrational state such that Ba+HI collisions with small impact parameter produce BaI with large vibrational excitation.

I. INTRODUCTION

Gas-phase reactions performed under single-collision conditions provide an excellent environment for the study of simple systems in very high detail and allow the determination of many different properties and experimental observables. The impact parameter is one quantity that cannot be measured directly and defies control in any type of gas-phase scattering experiments. It is defined as the distance of closest approach of two colliding particles in the hypothetical absence of any interaction between them. Information about it can only be inferred from the properties of the reaction products.[1] Its magnitude, b, is related to orbital angular momentum, L, through the expression

$$|\mathbf{L}| = \mu\,|\mathbf{v}_{\mathrm{rel}}|\,b, \tag{1}$$

where μ and $\mathbf{v}_{\mathrm{rel}}$ are the reduced mass and the relative velocity of the colliding particles. In the reaction

$$\mathrm{Ba+HI \rightarrow BaI+H} \tag{2}$$

the rotational angular momentum of the reagent HI is small compared to that found in the product BaI. The orbital angular momentum of the products is also relatively small.[2,3] In an isolated system total angular momentum is an invariant and therefore, conservation of angular momentum leads to the approximation

$$\mu\,|\mathbf{v}_{\mathrm{rel}}|\,b = |\mathbf{J}_{\mathrm{BaI}}|, \tag{3}$$

where $\mathbf{J}_{\mathrm{BaI}}$ is the rotational angular momentum of BaI, and its measure is given by

$$|\mathbf{J}_{\mathrm{BaI}}| = \hbar\sqrt{J(J+1)}. \tag{4}$$

Equation (3) provides a powerful link between spectroscopically observable product internal states and the conditions preceding the reactive collision. Given that impact parameters are uncontrolled, the reaction occurs from a range of b values, each weighted by $2\pi b$, and the product distributions supply information on the specific opacity functions, i.e., the reaction probability for specific product vibrational levels as a function of impact parameter averaged over all collision orientations. In this kinematically favorable situation the distribution of impact parameters that lead to reaction can thus be directly determined by measurement of the product rotational state distribution.

The BaI $C\,^2\Pi$–$X\,^2\Sigma^+$ electronic transition was used in our study to determine rotational population distributions. This band system was chosen because it has been the subject of detailed spectroscopic investigation. Nonetheless, its spectroscopy remains a challenge to the experimentalist, because of the high density of lines per branch, the small spacing between vibrational band origins (5.6 cm^{-1}), and the existence of six branches per spin–orbit subband. Laser induced-fluorescence (LIF) spectra are rotationally resolved only for some branches in the (0,0) band. Selectively detected laser-induced fluorescence (SDLIF) is used to reduce the spectral congestion. It is accomplished by dispersing the fluorescence and monitoring the signal generated by the band of choice.

The first study to determine specific opacity functions was done in our lab on the Ba+HI reaction under beam-gas conditions using SDLIF.[4] The v=8 level was chosen because it is near the maximum of the product vibrational distribution. That work showed the specific opacity function for v=8 to be narrow (FWHM=1 Å) with a peak at 2.6 Å. Later work done under crossed beam conditions, which provided a narrower relative velocity distribution, focused on v=0 because that could be studied with LIF.[2,3] The specific opacity function was found to be very narrow

[a]Present address: Department of Chemistry, Massachusetts Institute of Technology, Cambridge, Massachusetts 02139.
[b]Present address: Department of Chemistry, University of Southampton, Southampton, Hampshire, S09 5NH, United Kingdom.
[c]Author to whom correspondence should be addressed.

 0021-9606/92/227220-06$006.00

(FWHM=0.3 Å) and highly asymmetric with a peak near 4.5 Å.

In this paper, we report the rotational distribution of BaI in vibrational levels 0, 4, 8, 12, 16, and 18 formed under beam-gas conditions. These data, collected using SDLIF, are used to extract information on the impact parameter distributions that lead to the formation of these product vibrational levels.

II. EXPERIMENT

The experimental apparatus consists of a reaction chamber, a probe laser source, and a fluorescence detection system.[5] A radiatively heated stainless steel crucible is the main part of the differentially pumped oven chamber; it contains Ba metal and is maintained at approximately 1300 K to generate a collimated, neat Ba beam. A HI lecture bottle at 195 K delivers HI to the main reaction chamber via a needle valve; HI pressure is held between 4 and 8 $\times 10^{-4}$ Torr to ensure single-collision conditions in the probe region. Studies of the pressure dependence of the BaI ($v=0$) rotational distribution did not exhibit any relaxation for pressures as high as 1.0×10^{-3} Torr. The chamber temperature is 301 ± 3 K.

BaI product molecules are excited in the $C\,^2\Pi - X\,^2\Sigma^+$ band system using a single-mode cw ring dye laser pumped by an argon ion laser. The output beam is expanded and attenuated to approximately 23 mW cm^{-2} before intersecting the Ba beam at right angles. Low excitation power is required to avoid saturation of the C–X transition because of its large transition dipole moment. BaI fluorescence is imaged on the 250 μm wide by 50 mm high entrance slit of a 1 m monochromator[4,6] and detected with a photomultiplier tube. The signal is accumulated by photon counting as a function of laser wave number and stored in the computer that controls the laser.

The monochromator transmission spectrum is recorded using the same optics to collect very low power laser light scattered inside the chamber. Separate tests done using Ba $^1P^0$–^1S LIF show that these spectra match the true transmission function very closely.

Doppler-broadened spectra of the Ba ^3D–^1S transition are recorded by exciting the Ba atoms with a focused beam that intersects the atomic beam at 45° and collecting the fluorescence of the ^3D–^3P line through a bandpass interference filter.[5] In all cases, the I_2 $B\,^3\Pi_{0_u^+}$–$X\,^1\Sigma_g^+$ spectrum[7] and the laser power are recorded simultaneously for reference.

III. ROTATIONAL STATE DISTRIBUTIONS

Figure 1 shows the $\Delta v=0$ sequence of the BaI $C\,^2\Pi_{3/2}$–$X\,^2\Sigma^+$ excitation spectrum generated under beam-gas conditions.[8] This spectrum reflects the vibrational distribution of the reaction products because the Franck–Condon factors for the $\Delta v=0$ sequence are nearly unity.[9] This spectrum also shows the extensive overlap of the vibrational bands. To isolate one band, molecules are excited on one branch and fluorescence from two branches sharing

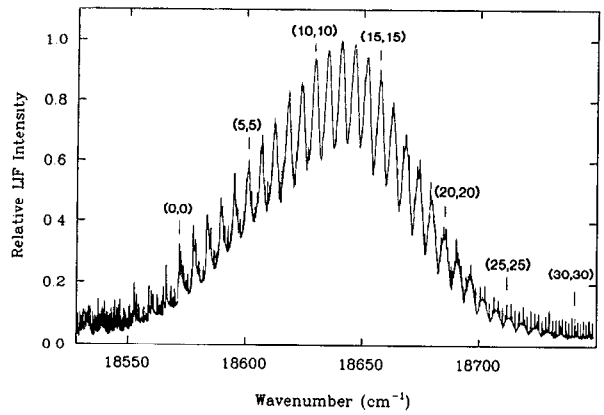

FIG. 1. The BaI $C\,^2\Pi_{3/2}$–$X\,^2\Sigma^+$ $\Delta v=0$ band sequence. BaI was produced in a beam-gas reaction of Ba+HI. The spectrum shown has been highly averaged to enhance the broadband features. The vibrational assignment of each band is indicated.

the same excited levels is selectively detected (SDLIF) by means of the monochromator (see Fig. 2).

The SDLIF scheme of excitation of the R_{21} branch and collection of the fluorescence from the P_{21} and Q_2 branches ($R_{21}\rightarrow P_{21},Q_2$) is preferred over the other possible scheme, i.e., $P_2\rightarrow Q_{21},R_2$. The preferred procedure requires stepwise recording of the rotational distribution, because one monochromator transmission spectrum cannot cover the whole distribution of the P_{21},Q_2 branch members without admitting fluorescence from unwanted bands. The advantage afforded by this scheme is that the inescapable coobservation of branches (Q_{21},R_2) belonging to neighboring vibrational bands crossing the branch of interest results in a sharp, almost continuous rise in the baseline and allows determination of the R_{21} line intensities. The other spin–orbit subband does not lend itself as efficiently to the determination of line intensities, because hyperfine splittings cause lines in the $C\,^2\Pi_{1/2}$–$X\,^2\Sigma^+(v,v)$ bands to be approximately twice as wide as in the $C\,^2\Pi_{3/2}$–$X\,^2\Sigma^+(v,v)$ bands.[10]

Figure 2(c) shows a representative example of a SDLIF scan using the monochromator transmission spectrum shown on the left of Fig. 2(b). All lines are easily assigned[11] and their intensities are measured above the local baseline. These intensities are converted to rotational populations by considering transition probabilities[12] for the excitation and emission step and the transmission probability through the monochromator. To facilitate this simple calculation as well as spectral simulations, monochromator transmission spectra are fit by the following function:

$$I(\sigma)=A(\sigma-p_1)^3\exp\left[-\left(\frac{\sigma-p_2}{p_3}\right)^2\right], \tag{5}$$

where $I(\sigma)$ is the transmission probability at the wave number σ and A, p_1, p_2, and p_3 are adjustable parameters.

The vibrational levels reported in this paper are 0, 4, 8, 12, 16, and 18. All experiments were done under similar conditions and one rotational population distribution for each vibrational level is shown in Fig. 3. No error bars are shown, but the scatter of the population of successive ro-

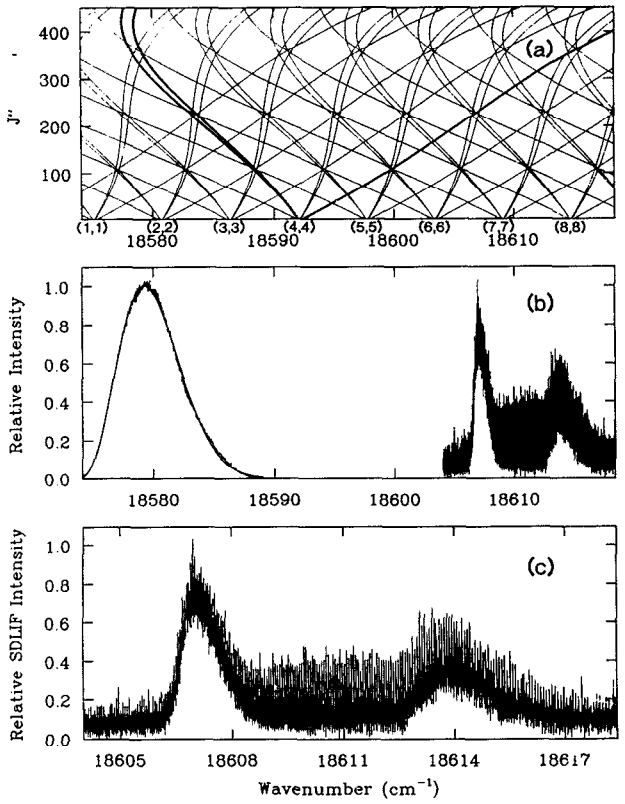

FIG. 2. (a) Fortrat diagrams for the BaI $C\,^2\Pi_{3/2}$–$X\,^2\Sigma^+$ $\Delta v=0$ sequence. The vibrational assignment is indicated at the origin of each band. Three branches of the (4,4) band sharing the same upper levels are highlighted. In order of increasing wave number, the branch labels are P_2, P_{21}, Q_2, Q_{21}, R_2, and R_{21}. (b) On the right-hand side, SDLIF spectrum of BaI $C\,^2\Pi_{3/2}$–$X\,^2\Sigma^+$ (4,4) R_{21} branch members, superimposed on the broad features caused by the BaI $C\,^2\Pi_{3/2}$–$X\,^2\Sigma^+$ (6,6) and (7,7) Q_{21}, R_2 branches. On the left-hand side, monochromator transmission spectrum chosen to collect preferentially fluorescence from the BaI $C\,^2\Pi_{3/2}$–$X\,^2\Sigma^+$ (4,4) P_{21} and Q_2 branches. The optimized simulation (smooth solid line) is based on the fitting parameters (and 1σ standard deviations) p_1 $=18573.39$ (2) cm^{-1}, $p_2=18571.07$ (11) cm^{-1}, and $p_3=4.02$ (2) cm^{-1} which correspond to a FWHM of 6.0 cm^{-1}. (c) Detailed view of the right-hand side of Fig. 2(b). The rotational quantum number, J, ranges from 177.5 to 396.5.

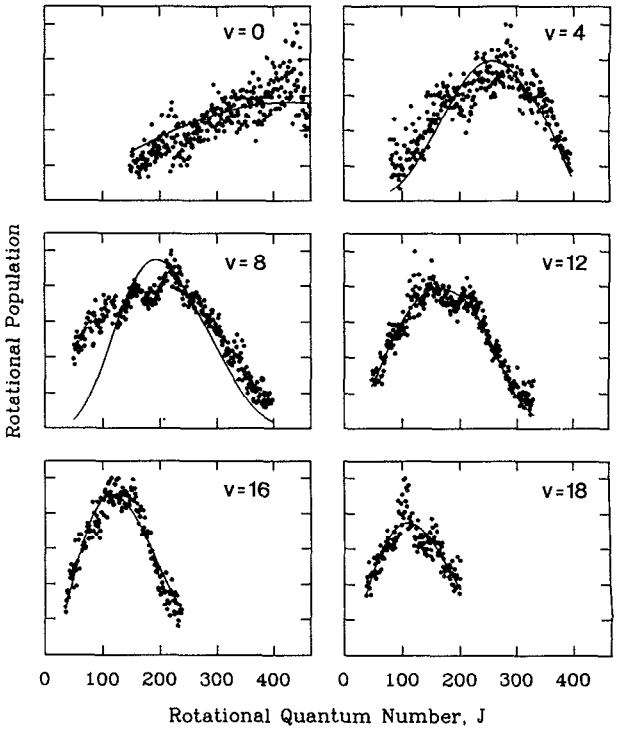

FIG. 3. BaI(v) beam-gas rotational distributions for the vibrational levels shown. The solid lines correspond to best fit simulations as described in the text.

tational states is indicative of the associated uncertainties. A clear trend can be seen from these data. The peak of the rotational distribution moves toward lower J values as the vibrational quantum number increases. Rotational distributions for v between 18 and 24 have very similar forms and no significant variation in the peak position can be seen.

The barium beam velocity distribution is determined through a fit[5] in which the line profile of the two-photon Ba $^3D_2$–$^1S_0$ transition is convoluted with the velocity distribution to simulate the experimental Doppler-broadened Ba spectrum. HI is assumed to follow a thermal Maxwell–Boltzmann distribution with a temperature equal to that of the reaction chamber. The relative velocity distribution is then calculated by convoluting the one-dimensional Ba distribution with the three-dimensional one of HI.[13] Figure 4 shows an example of all three distributions.

Our results for $v=8$ do not agree very closely with the earlier beam-gas work.[4] The origins of this discrepancy can be traced to differences in the way the experiments were done and in the way the data were processed which arises from improved understanding of the spectroscopy. Noda *et al.* [4] scanned over the P_{12} branch, used considerably higher laser power which broadened the line profiles and increased overlaps, implemented a less refined measurement of the Ba beam velocity distribution, and relied on a limited number of measurements of the monochromator

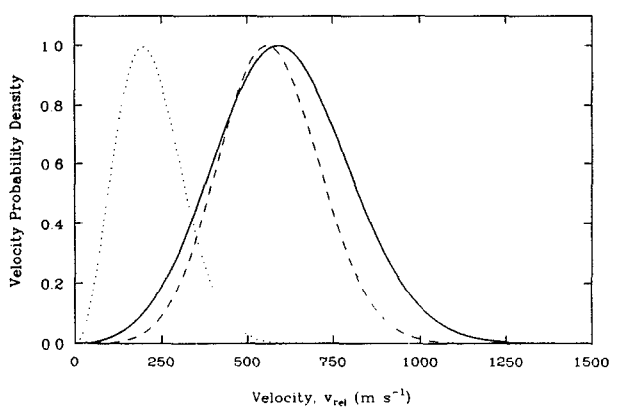

FIG. 4. Velocity distributions for the Ba and HI reagents in a beam-gas experiment. The dotted, dashed, and solid lines represent the distributions for HI, for Ba, and for the relative velocity respectively. The latter peaks at 590 m s^{-1} and has a FWHM of 460 m s^{-1}.

TABLE I. Most populated rotational states, mean internal energy, specific opacity function peaks and widths for the vibrational levels investigated. Values in parentheses are 1σ standard deviations.

v	J_{max}	E_{int} (kcal mol^{-1})	β_v (Å)	σ_v (Å)
0	418	9.6	4.5	0.2
4	286	7.1	4.23 (3)	0.36 (7)
8	220	7.4	2.92 (3)	1.0
12	150	7.9	2.52 (4)	1.53 (9)
16	127	8.4	1.85 (3)	0.97 (4)
18	106	8.9	1.2 (1)	1.3 (1)

transmission spectrum. In addition, subsequent spectroscopic studies[11] have improved our knowledge of the position of the branches used to collect the fluorescence and the ones that interfere with the observation.

IV. SPECIFIC OPACITY FUNCTIONS

The expression for the conservation of angular momentum [viz. Eq. (3)] is central to the extraction of the specific opacity function, $P_v(b)$, from the rotational distribution, $n_v(J)$, for a vibrational level v. This treatment assumes that (1) the rotational angular momentum in the HI reagent, $\mathbf{J}_{HI}$, is small relative to that in BaI (v), and (2) the orbital angular momentum of the products, $\mathbf{L}'$, is also small relative to the rotational angular momentum of BaI (v). The first condition is readily met because at room temperature 92% of the HI molecules have J_{HI} values less than or equal to 8. The second condition can be justified from energetic considerations. The Ba+HI reaction is slightly exoergic[5] (7.3 ± 2.0 kcal mol^{-1}), and the average collision energy is 3.1 kcal mol^{-1} with a FWHM of 4.0 kcal mol^{-1}. The available energy that can appear as product relative translation and BaI rotation is 10.4 ± 2.6 kcal mol^{-1} for BaI ($v=0$) and 1.6 ± 2.6 kcal mol^{-1} for BaI ($v=18$). As seen from Table I, almost all available energy is channeled into internal energy of the BaI product for the vibrational states investigated. Hence, condition (2) is also met. For example, if 3 kcal mol^{-1} is channeled into relative translational energy of the products, and a recoil impact parameter of 2 Å is assumed, then approximately 15 $\hbar$ is carried away in orbital angular momentum of the products. Furthermore, the omission of $\mathbf{J}_{HI}$ and $\mathbf{L}'$ is expected to make an average projection of zero on $\mathbf{J}_{BaI}$, assuming that these vector quantities are uncorrelated. Thus, the neglect of these small terms only has the effect of increasing the uncertainty in the magnitude of the reagent orbital angular momentum inferred from $|\mathbf{J}_{BaI}|$.

In what follows, we try to find a form of $P_v(b)$ which when convoluted with the relative velocity distribution, $f(v_{rel})$, will simulate the experimental $n_v(J)$.

$$n_v(J)=\int_0^\infty\int_0^\infty 2\pi b v_{rel}P_v(b)f(v_{rel}) \times\delta(J-\mu v_{rel}b/\hbar)db\,dv_{rel}. \quad (6)$$

The conditions imposed on the convolution integral arise from the conservation of energy and angular momentum.

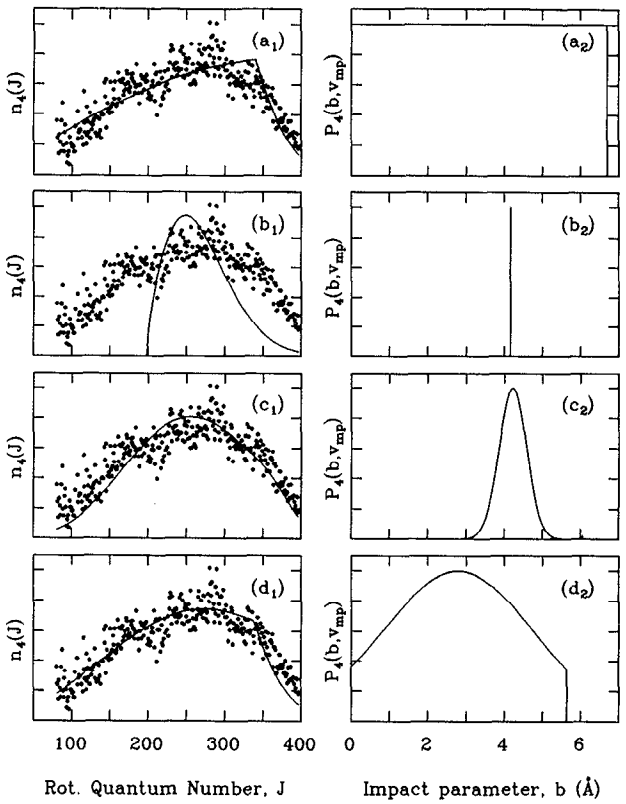

FIG. 5. Experimental and simulated BaI ($v=4$) rotational distributions and associated specific opacity function models. (a) Step function model: The only adjustable parameter was optimized to $D_0^0(\text{BaI})=80.20$ (6) kcal mol^{-1}. (b) Constant product recoil energy (CPR) model: The only adjustable parameter was optimized to $D_0^0(\text{BaI})-E_{rec}=75.38$ (6) kcal mol^{-1}. (c) Truncated Gaussian model: The adjustable parameters were optimized to $\beta_4=4.23$ (3) Å and $\sigma_4=0.36$ (7) Å, while D_0^0(BaI) was set to 78.1 kcal mol^{-1}. (d) Truncated Gaussian model with energy barrier: The adjustable parameters were optimized to $\beta_4=2.79$ (7) Å and $\sigma_4=2.0$ (1) Å, while D_0^0(BaI) was set to 78.1 kcal mol^{-1} and the energy barrier was set to 2.6 kcal mol^{-1} (allowing velocities greater than 574 m s^{-1} to be reactive).

Tests on the sensitivity of the data on the width of the opacity function were performed by considering two extreme cases. These tests were done on $v=4$ data and the results are shown in Figs. 5(a) and 5(b).

The simplest model describing collisions is the hard sphere model. This model has been proposed to describe the total opacity function.[15] Its functional form is

$$P(b)=H(b_{max}-b), \quad (7)$$

where $H(x)$ is the Heavyside (step) function and the limiting value for the impact parameter, b_{max}, is determined through energy conservation calculations.[3]

A nonlinear least-squares fit was performed on the BaI ($v=4$) data set with the bond dissociation energy of BaI, D_0^0(BaI), as the only adjustable parameter. The limitations of the model become apparent in Fig. 5(a). A narrower range of impact parameters is required to describe the data.

Noda and Zare[16] in a theoretical approach to the same reaction proposed a constant product recoil energy model (CPR). In this model the value of the impact parameter is calculated based on the solution of the simultaneous equa-

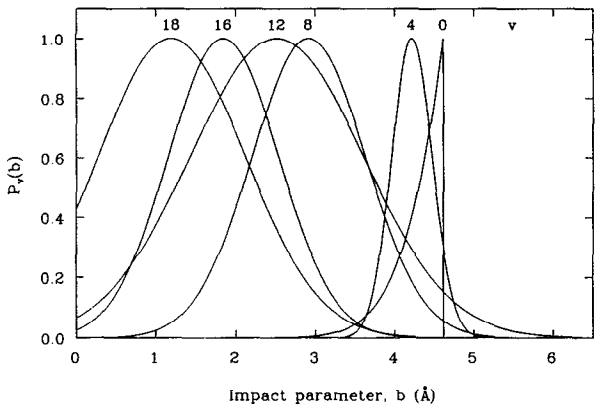

FIG. 6. Specific opacity functions of the Ba+HI reaction for the formation of BaI in the vibrational levels shown as derived from the data shown in Fig. 3 and explained in the text.

tions for the conservation of energy and angular momentum. A fit was performed using the same data with considerable success [see Fig. 5(b)]. The fact that the simulated rotational distribution was narrower than the experimental one suggested that a small but finite spread in the opacity function would improve the simulation.

A more sophisticated model was the so-called "truncated Gaussian" model which had been tried before.[3] The general form of the opacity function was a Gaussian which was truncated by the energetic limitations:

$$P_v(b)=\exp\left[-\frac{1}{2}\left(\frac{b-\beta_v}{\sigma_v}\right)^2\right]H[b_{\max}(v_{\rm rel})-b], \qquad (8)$$

where β_v and σ_v are fitting parameters different for each vibrational level v. No scaling factor has been included because all data are relative population distributions. The results for $v=4$ shown in Fig. 5(c) indicate a good agreement between the experimental data and the simulation.

A "static" energy barrier of 2.6 kcal mol^{-1} has been proposed in the past.[17] In an attempt to improve the fit further and test the existence of an energy barrier, all collisions occurring at energies less than 2.6 kcal mol^{-1} were considered nonreactive. The results shown in Fig. 5(d) indicate that no improvement was achieved with this addition. Thus, all rotational distributions were fit by using the simpler model in Eq. (8).

In an initial fitting procedure, σ_v in Eq. (8) was set equal to 0.2 Å for all v. The $v=4$ data gave a good fit, but for higher v values the simulated distributions were narrower than the experimental ones. The calculation for $v=0$ could not simulate the sharply peaked experimental distribution. σ_v was allowed to increase for higher v values until the simulations matched the data. The results are presented in Table I and in Figs. 3 and 6.

For high vibrational levels, the whole form of $P_v(b)$ is reactive, whereas for low vibrational levels a section on the high-b side is truncated by energy limitations. This statement is not made a priori, but is based on the trends seen in the rotational distributions. The decrease in rotational average energy is not matched by an equal increase in vibrational energy as higher vibrational levels are considered (see Table I). Two different explanations are possible: (1) recoil energy is higher for higher product vibrational states; or, (2) the average energy in a reactive collision that leads to formation of low vibrational levels is higher than the collision energy that leads to formation of higher vibrational levels. The latter hypothesis implies that different sections of the relative velocity distribution are reactive for different product levels.

For the lowest vibrational level, some mechanism needs to be assumed that truncates a large, low-velocity section of the relative velocity distribution to explain the unexpectedly high rotational excitation observed. A static activation energy barrier is not confirmed by the other vibrational level distributions. A centrifugal barrier[13] is a more plausible explanation, but the fit is not very satisfactory. It is very interesting to note that the BaI ($v=0$) rotational distribution generated under beam-gas conditions is similar to that seen under crossed-beam conditions,[3] where the average relative velocity was much higher, approximately 950 m s^{-1} compared to 590 m s^{-1}.

No satisfactory explanation can be given for the (unexpectedly) high rotational excitation of BaI ($v=0$). In any event, the data confirm that BaI ($v=0$) is formed under beam-gas conditions at impact parameters that are at least as high as those determined in the crossed-beam studies.[3] This argument was the underlying spirit in the construction of Fig. 6. For $v\geqslant 4$, the opacity functions shown are determined from beam-gas experimental data and that for $v=0$ from crossed-beam data.

The earlier work[4] on $v=8$ had shown a similar trend for the shape and the position of $P_8(b)$, although the specific results differ for reasons outlined in the previous section.

Using a LEPS potential for the BaIH surface, Zhao and Zare carried out quasiclassical trajectory calculations for this reaction.[18] Among the conclusions reached, $P_v(b)$ is found to be a narrow function of b and to overlap neighboring vibrational levels. Moreover, $P_v(b)$ is unimodal with the b value of the peak decreasing with increasing v, so that the $P_v(b)$ functions form a nested set. The results of the present study are in qualitative agreement with this simulation.

V. CONCLUSIONS

Beam-gas experiments do not provide very narrow relative velocity distributions or product state distributions. Yet, rotational population distributions, $n_v(J)$, recorded for BaI($v=0$, 4, 8, 12, 16, 18) show remarkable trends. As v increases, $n_v(J)$ changes from a sharply peaked function at very high J values (e.g., $J=438$) for $v=0$ to a broad distribution with a maximum near $J=100$ for $v=18$.

The corresponding specific opacity functions are not very well determined, but reflect a similar trend. $P_0(b)$ is a function sharply peaked at the energetic limit of the system with $b=4.5$ Å. At higher vibrational levels, $P_v(b)$ becomes broader, more symmetric, and its peak value decreases. The implication is that the vibrational state in which BaI is formed is determined primarily by the impact parameter of

the collision between Ba and HI, although the collision velocity and the orientation angle are expected to have some effect. A 1:1 mapping is found in which reactive collisions with large impact parameters correspond to BaI product in low states of vibrational excitation. This mapping becomes less faithful for higher vibrational levels where the specific opacity functions overlap extensively.

Seen from a different perspective the present study provides a measure of atomic and molecular sizes. The apparent size of a Ba atom approached by a HI molecule is a function of the vibrational state BaI that will be formed.

The impact parameter values found can be compared with the equilibrium bond length of BaI, viz. 3.08 Å, which remains largely the same at the vibrational or rotational levels under consideration. Clearly, the reaction starts taking place well before Ba and I have reached their final configuration.

This study has exploited the extreme case of a kinematically constrained system to deduce the nature of the specific opacity function. Additional work is needed to elucidate the character of the reaction barrier and its relation to product vibrational states, to provide an explanation for the unexpected behavior of the BaI ($v=0$) rotational distributions, and reveal the dependence of the reaction probability on the relative velocity. Such detailed information should become available from crossed-beam studies of the same reaction. The same technique should also be applicable to less kinematically constrained reactions to uncover the hidden role of the impact parameter in a chemical reaction.

ACKNOWLEDGMENTS

We thank P. H. Vaccaro for helpful discussions and S. V. Filseth for helpful comments on the manuscript. C. A. L. thanks the SERC for a NATO postdoctoral fellowship. This work was supported by National Science Foundation under Grant No. NSF CHE-89-21198.

[1] D. R. Herschbach, Faraday Discuss. Chem. Soc. **33**, 281 (1962); D. R. Herschbach, Adv. Chem. Phys. **10**, 319 (1966).
[2] C. A. Leach, A. A. Tsekouras, P. H. Vaccaro, R. N. Zare, and D. Zhao, Faraday Discuss. Chem. Soc. **91**, 183 (1991).
[3] P. H. Vaccaro, A. A. Tsekouras, D. Zhao, C. A. Leach, and R. N. Zare, J. Chem. Phys. **96**, 2786 (1992).
[4] C. Noda, J. S. McKillop, M. A. Johnson, W. R. Waldeck, and R. N. Zare, J. Chem. Phys. **85**, 856 (1986).
[5] P. H. Vaccaro, D. Zhao, A. A. Tsekouras, C. A. Leach, W. E. Ernst, and R. N. Zare, J. Chem. Phys. **93**, 8544 (1990).
[6] D. Zhao, P. H. Vaccaro, A. A. Tsekouras, C. A. Leach, and R. N. Zare, J. Mol. Spectrosc. **148**, 226 (1991).
[7] S. Gerstenkorn and P. Luc, *Atlas du Spectre de la Molécule d'Iode* (Centre National de la Recherche Scientifique, Paris, 1978); S. Gerstenkorn and P. Luc, Rev. Phys. Appl. **14**, 791 (1979).
[8] P. H. Vaccaro, D. Zhao, A. A. Tsekouras, and R. N. Zare (unpublished results).
[9] P. J. Dagdigian, H. W. Cruse, and R. N. Zare, J. Chem. Phys. **60**, 2330 (1974).
[10] W. E. Ernst, J, Kändler, C. Noda, J. S. McKillop, and R. N. Zare, J. Chem. Phys. **85**, 3735 (1986); C. A. Leach, W. E. Ernst, J. Kändler, C. Noda, J. S. McKillop, and R. N. Zare, *ibid.* **95**, 9433 (1991).
[11] C. A. Leach, A. A. Tsekouras, and R. N. Zare, J. Mol. Spectrosc. **153**, 59 (1992).
[12] R. N. Zare, *Angular Momentum: Understanding Spatial Aspects in Chemistry and Physics* (Wiley, New York, 1988).
[13] R. C. Estler and R. N. Zare, Chem. Phys. **28**, 253 (1978); A. E. Redpath, M. Menzinger, and T. Carrington, *ibid.* **27**, 409 (1978).
[14] R. D. Levine and R. B. Bernstein, *Molecular Reaction Dynamics and Chemical Reactivity* (Oxford University, New York, 1987).
[15] A. Siegel and A. Schultz, J. Chem. Phys. **76**, 4513 (1982).
[16] C. Noda and R. N. Zare, J. Chem. Phys. **86**, 3968 (1987).
[17] C. A. Mims, S.-M. Lin, and R. R. Herm, J. Chem. Phys. **57**, 3099 (1972).
[18] D. Zhao and R. N. Zare, J. Chem. Phys. **97**, 6208 (1992).